Absolute keV X-ray yield and conversion efficiency in over dense Si sub-petawatt laser plasma

Sergey N. Ryazantsev[1,2,*], Artem S. Martynenko [2,3], Maksim V. Sedov[2], Igor Yu. Skobelev[1,2], Mikhail D. Mishchenko[2,4], Yaroslav S. Lavrinenko[1,5], Christopher D. Baird[6], Nicola Booth[7], Phil Durey[6], Leonard N. K. Döhl[6], Damon Farley[6], Kathryn L. Lancaster[6], Paul McKenna[8], Christopher D. Murphy[6], Tatiana. A. Pikuz[2,9], Christopher Spindloe[7], Nigel Woolsey[6] and Sergey A. Pikuz[1,2]

[1]National Research Nuclear University MEPhI (Moscow Engineering Physics Institute), 115409 Moscow, Russia

[2]Joint Institute for High Temperatures of the Russian Academy of Sciences, Moscow 125412, Russia

[3]Plasma Physics Department, GSI Helmholtzzentrum fur Schwerionenforschung, 64291 Darmstadt, Germany

[4]European XFEL, 22869 Schenefeld, Germany

[5]Moscow Institute of Physics and Technology, State University, 141701 Moscow, Russia

[6]York Plasma Institute, Department of Physics, University of York, York YO10 5DD, United Kingdom

[7]Central Laser Facility, STFC Rutherford Appleton Laboratory, Didcot OX11 0QX, United Kingdom

[8]Department of Physics, SUPA, University of Strathclyde, Glasgow G4 0NG, United Kingdom

[9]Open and Transdisciplinary Research Initiative, Osaka University, Osaka 565-0871, Japan

E-mail: *SNRyazantsev@mephi.ru

Abstract. Laser-produced plasmas are bright, short sources of X-rays commonly used for time-resolved imaging and spectroscopy. Their usage implies accurate knowledge of laser-to-X-ray conversion efficiency, spectrum, photon yield and angular distribution. Here we report on soft X-ray emission in the direction close to the target normal from a thin Si foil irradiated by a sub-PW picosecond laser pulse. These absolute measurements cover a continuous and broad spectral range that extends from 4.75 to 7.5 Å(1.7–2.6 keV). The X-ray spectrum consists of spectral line transitions from highly charged ions and broadband emission with contributions from recombination and free-free processes that occur when electrons decelerate in plasma electromagnetic fields. Angular distribution of the emission was investigated via PIC simulations, which allowed to estimate the yield into the full solid angle. We found that experiment and simulation estimations of laser to free-free emission conversion efficiency are in a good agreement.

1. Introduction

Plasmas produced by irradiation of different objects (flat foils [1, 2, 3], microstuctured surfaces [4, 5], wavelength-scale spheres [6], velvet surfaces [7], nanowires [8, 9], gas jets [10, 11, 12]) by intense laser pulses (Laser Produced Plasma, referred below as LPP) are widely used as an X-rays sources for both fundamental and applied research.

This is due to the possibility to precisely synchronise a measurement with phase of evolution of aprobed object and the relatively short duration of the emission. When nanosecond pulses are used, it is usually equal to their duration [13] and, in the case of picosecond pulses, exceeds it not by more than two orders of magnitude depending on laser intensity [1] or target type [7]. It should be noted, however, that the radiation from plasma sources generated by femtosecond pulses also can lasts up to several picoseconds [14]. Broadband emission sources are often needed for bioimaging and absorption spectroscopy. LPP at the table-top scale are used as X-ray sources in commercial applications [15] and at the very large scale in inertial confinement fusion (ICF) research as very bright X-ray backlighters for capsule explosions. Petawatt-class (PW) lasers facilities (such as ARC [16] and PETAL [17] or others mentioned at TABLE E.1 in [18]) which can produce picosecond pulses of about kJ are used for these purposes. Even for ICF experiments sources of soft X-rays are required. For example, low energy photons of <2 keV are used for the backlighting of direct-drive cryogenic DT implosions [19] due to the low opacity of the plastic shell and the deuterium-tritium fuel [20]. In addition, the low energy part of the spectrum of PW short-duration plasma sources spectrum is used to study warm-dense-matter by absorption spectroscopy [21].

These two applications, the imaging of an ICF experiment and diagnosis of warm-dense-matter, require a different spectral composition of the probe radiation. A source with a narrow emission band, ideally monochromatic, is required to acquire high-quality backlit images. Absorption spectroscopy, on the other hand, is most effective when using a radiation source with a continuous spectrum without spectral line features or sharp drops in intensity [22]. Both types of the probe radiation can be obtained using LPP due to different processes, which are shown in Fig. 1.

Plasma ions produce characteristic spectral lines during transitions of electrons between bound energy levels. For highly charged ions even with relatively low-Z (around 10) the lines are in the keV range of photon energy. Usually transitions from the excited state with principal quantum number n = 2 to the ground state in hydrogen-like (Ly_α) and helium-like transition (He_α) is at the appropriate wavelength for high-contrast quasi-monochromatic backlighting imaging [20, 23]. The plasma spectrum also contains lower intensity continuous emission from free-bound (photorecombination) and free-free (bremsstrahlung and synchrotron emission) transitions. Contributions of the individual process depend on element and irradiation conditions. Therefore a significant experimental effort is required to characterize LPP sources including those produced by picosecond PW pulses.

In this work we investigate the soft X-ray emission properties of a near solid density

Absolute keV X-ray yield and conversion efficiency in over dense Si sub-petawatt laser plasma 3

plasma generated in a Si foil by a sub-PW laser pulse. The aim of the work is to present exact values for the X-ray source photon yield in absolute units in the direction close to the target normal and briefly describe physical processes that contribute to the emission.

2. Experimental setup

The experimental investigation of the emissivity in soft X-ray range as a relativistic-intensity picosecond duration laser pulse strikes a Si foil was performed on Vulcan PW laser facility [24]. A schematic representation of the experimental setup is shown in Fig. 1. The plasma was created by irradiating 2 μm thick Si foils by pulses of p-polarised laser radiation with wavelength $\lambda = 1.054$ μm. Duration of the pulses was τ =1 ps. The beam was focused by an off-axis parabolic (OAP) mirror to a spot with a diameter of $\approx$7 μm. Initial (measured before the compressor) energy of the used pulses was $\approx$350 J, but only about 60% ($\approx$210 J) of it reached the target surface due to losses in different parts of the beam optical path including a plasma mirror [25] applied to enhance the laser pulse temporal contrast. The indicated parameters values corresponds to the pulse power P=0.2 PW and intensity I=3×10^{20} W/cm^2.

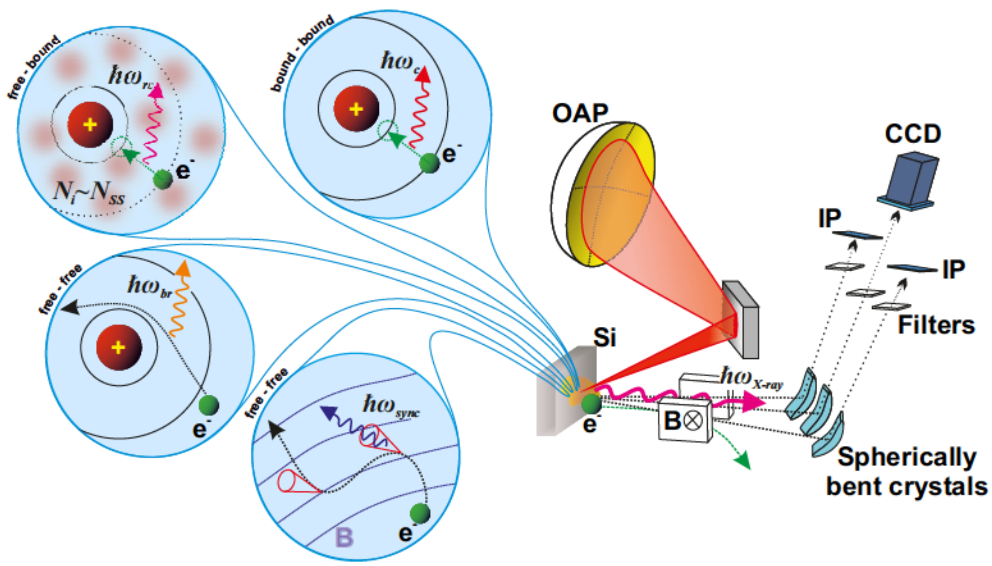

Figure 1. Experimental setup and schematic of the processes that form the shape of the plasma soft X-ray radiation spectrum registered in the experiments.

X-rays emitted from the front of the target during one laser shot was registered with three focusing spectrometers with spatial resolution (FSSR) [26] installed in directions close to the surface normal. Spherically bent α-quartz crystals with Miller indexes *(hkl)* (100) (interplanar spacing 2d = 8.512 Å) and (101) (2d = 6.666 Å) were used as disperse elements for them. Two FSSRs with the (100) crystals observed the overlapping wavelength ranges 5–6.8 Å and 6.5–7.4 Å. The third one with the (101) crystal was aligned to register photons with wavelength from 4.75 to 6 Å. Dispersion schemes chosen for the spectrometers provided spectral and spatial resolution of $\lambda/\Delta\lambda \approx 0.5 \times 10^4$

and ΔX ≈100 μm/pixel correspondingly. All the spectrometers were shielded against spurious radiation generated by the electrons from the interaction point as they hit the chamber walls, optical posts and so on. Two of the FSSRs were in housings made of 5 mm lead with small windows in the direction of the target crystal. The third FSSR was installed in a separate vacuum chamber connected to the main chamber by a narrow tube with its axis oriented towards the target. Also 0.5 T neodymium-iron-boron permanent magnets were installed between the FSSR crystals and the interaction point. As a result, the electrons accelerated towards the crystals could not reach them if their kinetic energy was less than 50 MeV. Fujifilm BAS-TR image plates (IP) and Andor CCD DX-434 (only for one of the spectrometers) were used as X-ray detectors. The IPs were covered by two layers of 1 μm thick polypropylene $(C_3H_6)_n$ with a thin (0.2 μm) layer of Al evaporated on it or by 25 μm thick beryllium film. The CCD sensor was shielded by a 25 μm Be foil for all the shots. The slits of the magnets were also covered by a single layer of 5 μm Mylar $(C_{10}H_8O_4)$ to avoid detector saturation.

The spectrometers observation ranges overlap to provide cross-calibration between the FSSRs. This enabled the measurement of continuous and high-resolution spectra over photon wavelengths from 4.7 to 7.3 Å(1.7 to 2.6 keV). The raw spectra registered by the individual FSSR spectrometers are shown in Fig. 2(a).

All data registered with the FSSRs were corrected for filtering, crystal reflectivity and detector response functions. Reflectivity was calculated by numerical modelling as described in [27] by ray tracing through the spectrometer. The actual crystallographic rocking curves of the spherically bent crystals installed in the FSSRs were used for it. They were calculated with the software XOP [28] and presented in Appendix together with sensitivity functions of the IPs. Transmission functions for the filters foils were calculated using the Henke tables [29]. A summary of the response functions for each spectrometer is shown in 2(b). After convolution of the registered signal with them an initial plasma radiation spectrum shape was restored (Fig.2(c)). Consideration of the equipment responce function allowed to scale the intensity (vertical axis in the figure) in absolute units of photons/$\AA$/sr. Thus it represents the emissivity of the source radiation in the direction of the spectrometers crystals (close to the targets normal). The most significant corrections were needed around the Si K-edge at 6.7135 Å[30]. This causes a drop in reflectivity of the α-quartz (SiO_2) crystals in the wavelength range close to the He_α line.

3. Discussion

The spectrum shown in Fig. 2(c) contains both characteristic and continuous emission components. Its shape is formed by all types of electron transitions: free-free, free-bound, bound-bound (Fig. 1). The characteristic emission of plasma ions is produced by transitions between energy states of H- and He-like Si ions. All the corresponding spectral lines are broadened due to the strong Stark effect. Their experimental shape is correctly reproduced (Fig. 3) by a theoretical spectrum simulated for the plasma

(a)

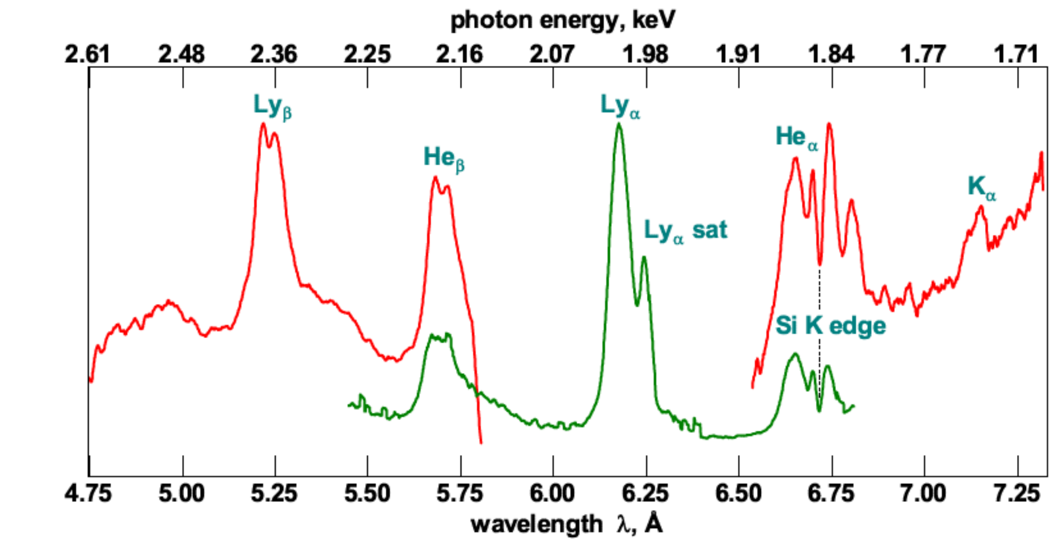

(b)

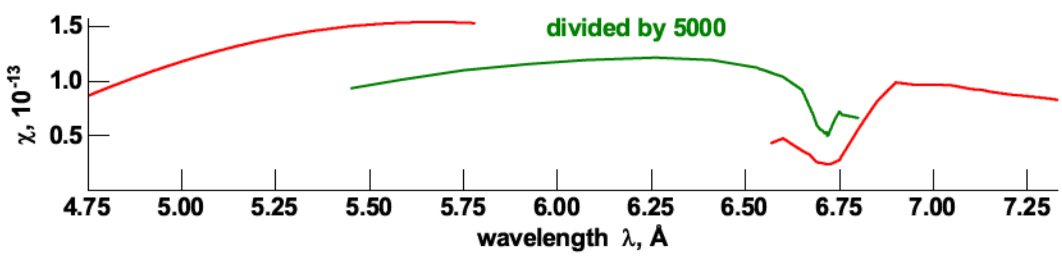

(c)

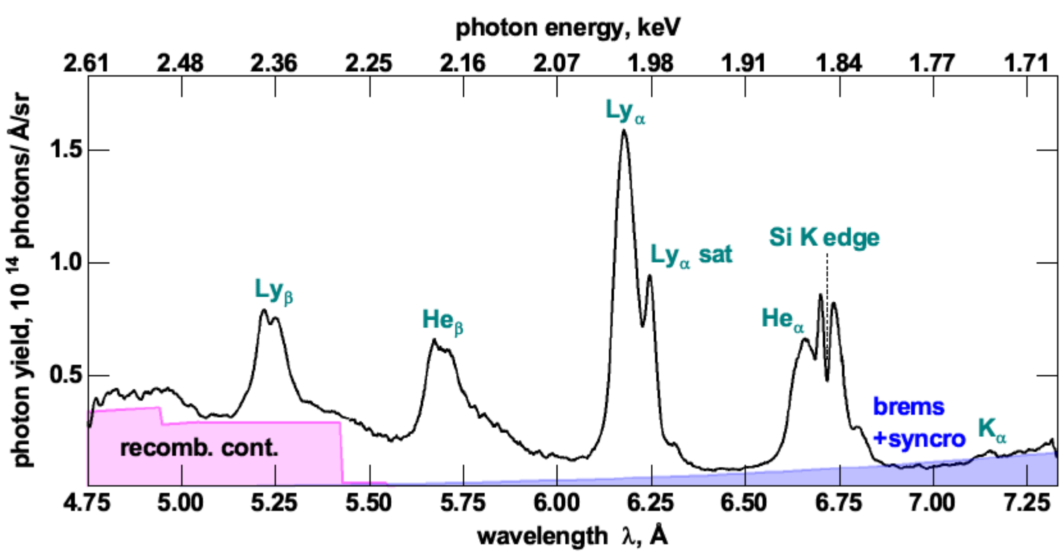

Figure 2. (a)—normalized experimental emission spectra registered by the FSSRs from the front side of Si foil before convolution with the spectrometer routes response functions $\chi(\lambda)$ shown in (b). $\chi(\lambda)$ is a ratio of the number of registered photons of λ wavelength to the one emitted by the source. (c)—combined experimental emission spectrum after convolution with $\chi(\lambda)$. The blue and purple polygons qualitatively demonstrate contributions of bremsstrahlung, synchrotron emission and recombination continuum. Shape of the latter one was calculated for solid-state Si plasma (N_i = $6{\times}10^{22}$ cm^{-3}).

electron temperature T_e=650 eV and electron density of 4×10^{23} cm^{-3}, which is about 60% of Si solid density value $N_{SS} \approx 6\times10^{23}$ cm^{-3}. It was achieved due to the extremely high value of the laser pulse temporal contrast of 10^{10} additionally enhanced by the plasma mirror.

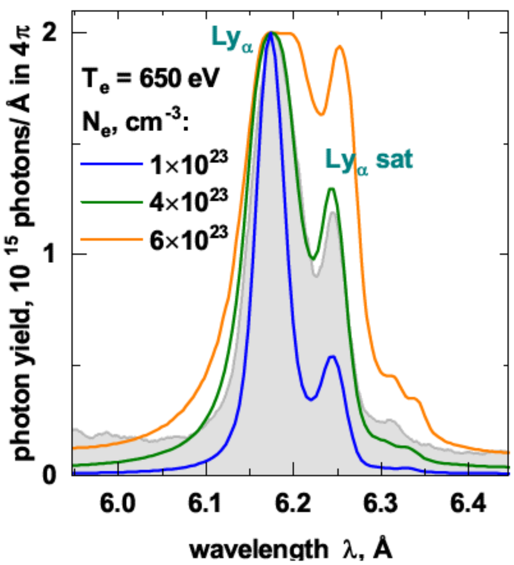

Figure 3. Comparison of Ly_α line shape registered in the experiments with that calculated theoretically for the fixed electron temperature T_e=650 eV and different ion densities: $N_e= 1\times10^{23}$ (blue line), 3×10^{23}(green) and 5×10^{23} cm^{-3}(orange). For the calculations it was assumed that the plasma has a linear size of 3 μm. The simulated spectra were obtained with PrismSPECT software [31].

The most intense line is the Ly_α (2p$\rightarrow$1s transition in an H-like ion). Emissivity of the source in this line (the narrow wavelength range from 6.05 to 6.35 Å, 1.95–2.05 keV, which contains the line itself and its dielectronic satellites) in the direction close to the targets normal is about 1.7×10^{13} photons/sr. This part of the plasma spectrum is best suited for implementation of quasi-monochromatic backlights schemes. The value for the broad peak indicated in the figure as He_α (range from 6.53 to 6.89 Å,1.8–1.9 keV) is $\approx 0.8\times10^{13}$photons/sr. Actually this spectral region contains overlapping He_α (1s2p $^1P_1$ $\rightarrow$1s2 $^1S_0$ in He-like ions), intercombination line (1s2p $^3P_{2,1}$ $\rightarrow$1s^2 $^1S_0$) and dielectronic satellites emitted by Li-like ions. Note that the peak to the left of the intensity drop caused by the K-edge is not the intercombination line. This is an artefact of registration previously observed for the spectrometers used in the experiments. Emissivities of the source in the Ly_β (3p$\rightarrow$1s) and He_β(1s3p $^1P_1$ $\rightarrow$1s^2 $^1S_0$) lines are 0.4×10^{13} and 0.6×10^{13} photons/sr respectively. In comparison the K_α line at 7.12 Å is weak as most of the Si is highly ionised. The indicated numbers correspond to a conversion efficiency (CE) of laser pulse energy to He_α, Ly_α, Ly_β, He_β lines emission in the direction close to the target normal as $\approx1.2\times10^{-5}$ sr^{-1}, $\approx2.5\times10^{-5}$ sr^{-1}, $\approx0.75\times10^{-5}$ sr^{-1}, $\approx1.0\times10^{-5}$ sr^{-1} respectively.

In the short wavelength part of the spectrum there is a pedestal. It results from the recombination continuum produced by free-bound transitions of plasma electrons. Spectral lines corresponding to 4p→1s transitions in H- and He-like ions should be registered in this range, but they are supressed due to ionization potential depression [32] in the dense plasma. The shape of the recombination continuum calculated using the Hummer-Mihalas [33] model for He- and H-like ions in a solid-density Si plasma is shown in Fig. 2(c) by the magenta area. Simulations indicate that the recombination continuum extends to 2 Å. Quite high yield (average value is $\approx 3\times10^{13}$ photons/Å/sr) value and absence of any spectral lines makes the recombination continuum part of the spectrum very suitable for X-ray absorption spectroscopy in the range $\leq$5 Å.

Another part of the continuous emission arose from free-free processes. They contribute to the spectrum through a monotonic growth in intensity in the long wavelength part. It is approximated by an exponential function shown by the blue line in Fig.2(c). An area under this curve gives an estimation for an amount of energy associated with free-free emission is E_{cont}=5 mJ/sr E_{cont}, which corresponds to CE of 2.5×10^{-5} sr^{-1}.

It is also possible to estimate a ratio $CE_{4\pi}$ of the energy emitted in the full solid angle 4π to the energy of the incident laser pulse. For bremsstrahlung and synchrotron emission it can be done semi-analytically on the base of electron energy distribution numerically obtained by particle-in-cell (PIC) simulations. We have performed two-dimensional (2D) PIC simulation via the EPOCH [34] code.

All the modelling parameters were chosen close to experimental conditions: laser wavelength $\lambda_{laser} = 1.054\ \mu$m, focal spot radius 4 μm, angle of incidence α=45°, intensity I_{las}=3×10^{20} W/cm^2. The laser pulse had Gaussian spatial and 3rd order super-Gauss temporal profile (Fig.4(a)). A 2 μm thick layer of fully ionized Si ions with solid-state density (5×10^{22} ions/cm^{-3}) was used as a target. A long laser pulse requires a large simulation box to accurately describe the laser-target interaction and to accommodate the expanding plasma. In our simulations the box size was $120\times120\ \mu$m with 10×10 nm grid. The simulation included a current smoothing algorithm and third order particle weighting to limit noise and numerical heating. All boundary conditions were absorbing for radiation and thermalizing for particles.

For an accurate description of the interaction of a laser pulse with a solid target, it is necessary that the minimum achievable particle density in the calculation (1 macro particle in 1 cell) be less than the critical density. On the other hand, at the edge of the simulation area particles will never interact with the laser pulse. They are needed only to maintain the quasi-neutrality of the plasma via the return current. Specifying a large number of macro particles for all cells in the target is a waste of computational resources. Therefore, in order to save computational time, the target was conditionally divided into several zones (Fig. 4(b)). Central zone 1 had 50 macro ion particles and 50×14 macro electron particles (1 macro electron in 1 cell corresponds to 0.9 n_{cr}) in each cell, zone 2 had half the number of macro particles in each cell (25 ions and 25×14 electrons) and zone 3 had 10 macro ion particles and 10×14 macro electron particles in each cell, respectively. The boundary of zone 1 was chosen from the condition that during the simulation time ($\tilde{1}.1$ ps) the electrons from zone 2 did not reach the focal spot.

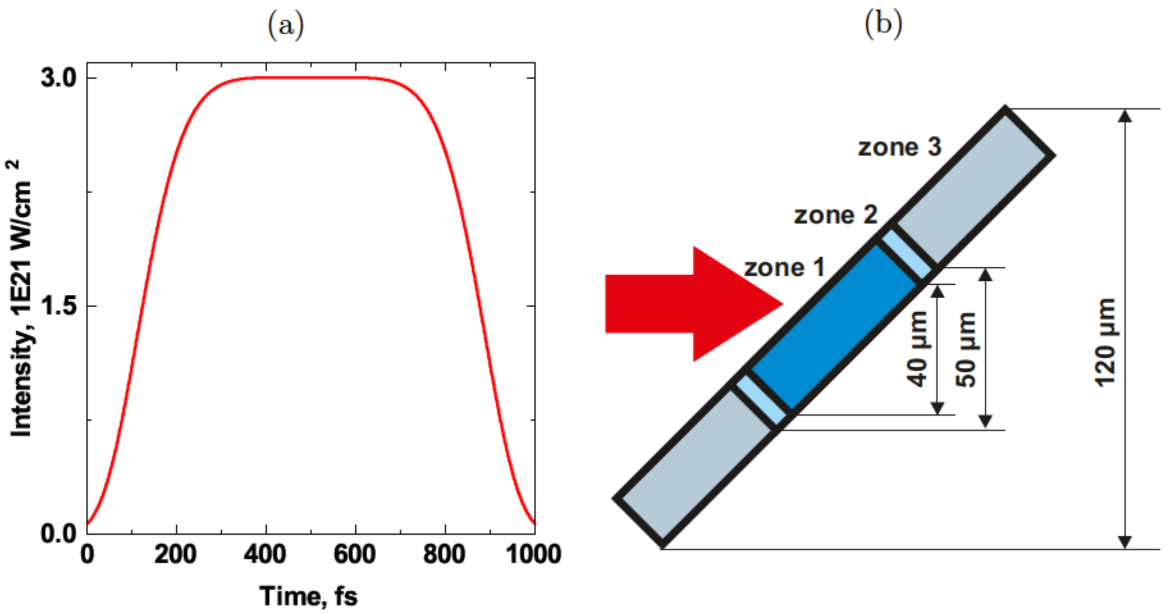

Figure 4. (a)—Temporal profile of the laser pulse used in PIC simulations. (b)—Scheme of dividing the target into zones with different numbers of macroparticles

The electron energy spectrum predicted by the PIC simulations is shown in Fig. 5(a). It can be roughly reproduced by a sum of three Maxwell distributions with temperatures of 5, 80 and 650 keV and electron densities $N_e = 3\times10^{13}$, 9×10^{13}, 1.5×10^{13} cm^{-3} respectively. On the base of these values it is possible to estimate amount of energy emitted as Bremsstrahlung and synchrotron radiation using modified Kramers formula (1) from [35] and the classical expression (2) from [36] correspondingly:

$$dI_{Brems}(E) = C\frac{Z^2 N_i n_e}{\sqrt{T_e}}\exp(-\frac{E}{T_e})dE; C = \frac{16}{3}\sqrt{\frac{2\pi}{0.5}}\frac{e^6}{m_e^{3/2}c^3}, \quad (1)$$

$$dI_{syncro}(E) = \frac{\sqrt{3}}{2\pi}\frac{e^3 H}{m_e c^2}F(\frac{E}{E_c})dE; F(\xi) = \int_{\xi}^{\infty} K_{\frac{5}{3}}(\xi)d\xi, \quad (2)$$

where Z—atomic number of the target atoms, N_i—ion density (6×10^{22} cm^{-3}), n_e—number of electrons, T_e—electron temperature in eV, g^{ff}—Gaunt factor, e and m_e—electron charge and mass, c—speed of light, H—magnetic field (considered as constant calculated as $\sqrt{\frac{2I}{c}}$=4.5×10^8 G), K is the modified Bessel function of the second type and E_c is an energy around which the emission of an electron with energy T_e is concentrated:

$$E_c = \hbar\omega_c; \omega_c = \frac{3eH}{2m_e c}\left(\frac{T_e}{m_e c^2}\right)^2. \quad (3)$$

It should be noted that according to (3) only electrons with energy $\geq$6 MeV make a significant contribution in the energy range detected by our spectrometers.

Integrating of (1) and (2) over the range of photon energies observed in the experiments gives the values of 0.1 J and 0.3 J for the Bremsstrahlung and synchrotron emission respectively. Dividing by the energy of the laser pulse used in the experiment (210 J) gives CE $_{4\pi}$ values η_{Brems}=3.3×10^{-4} and η_{syncro}=1×10^{-3}. The EPOCH code itself able to simulate spectrum (Fig. 5(b)) and angular distribution (Fig. 5(c)) of bremsstrahlung and synchrotron emission on the base of principles described in [37, 38, 39] and predict values for CE$_{4\pi}$. It gives $\eta^{4\pi}_{Brems} = 3.4\times10^{-4}$ and $\eta^{4\pi}_{syncro}$=1.3×10^{-4}. Such a significant discrepancy for the synchrotron emission CEs is caused by using a fixed value of the magnetic field for the analytical estimation based on the (2).

The predicted by PIC simulations angular distribution (Fig.5(c)) is not isotropic, because absorption within the target occurs in the direction parallel to the surface of the target (45° to 235° direction). The simulated distribution together with the experimental value for the energy of the emission associated with free-free transitions registered by the spectrometers allows to estimate the total energy emitted by the source in full solid angle 4π as bremsstrahlung and syncrotron emission. The obtained values is E$_{cont}$ ≈33 mJ, which is ≈52% of that obtained assuming an isotropic angular distribution. The corresponding CE$_{4\pi}$ value is 1.6×10^{-4}, which is about three times less than predicted by the PIC simulation. Impacts of the two types of free-free emission are indistinguishable in the experimental spectrum. Therefore, it is impossible to give separate estimates for their CEs. Nevertheless, according to the PIC results syncrotron emission should be less intense than bremsstrahlung for all the directions and the E$_{cont}$ is distributed between them as 1:2.6.

It can be assumed that the angular distribution for the line emission of the source also has a "dipole" shape. Under this assumption it is possible to estimate CE$_{4\pi}$ in separate spectral lines. The values are ≈0.8×10^{-4}, ≈1.6×10^{-4}, ≈0.5×10^{-4}, ≈0.5×10^{-4} for He$_\alpha$, Ly$_\alpha$, Ly$_\beta$, He$_\beta$ respectively. It the presented values are comparable with results reported by other research groups. For example, in experiments with Ag/Cu foils [40, 41] carried out at the same laser facility but under slightly different conditions, values of 1–2×10^{-4} were obtained for the spectral lines Ag K$_\alpha$ (E$_{ph}$=22.4 keV, λ = 0.553 Å) and Cu K$_\alpha$ (E$_{ph}$=1.54 keV, λ = 8.04 Å).

4. Conclusions

The laser plasma produced by the sub-PW (1 ps, 210 J, 210 TW, with focal spot diameter 7 μm, and on target intensity 3×10^{20} W/cm^2, angle of incidence is 45 ∘) laser pulse in a 2 μm thick Si foil is a very bright source of soft X-rays. In the direction close to the targets normal we registered emissivity of ≈8×10^{13} photons/sr (≈0.03 J/sr) in the wavelength range of 4.75–7.3 Å (1.7–2.6 keV), which corresponds to the conversion efficiency of ≈1.2×10^{-4} sr^{-1} . About half of the energy were emitted in Si XIV (Si^{13+}) Ly$_\alpha$, Ly$_\beta$ and Si XIII (Si^{12+}) He$_\alpha$ and He$_\beta$ resonance spectral lines and its dielectonic satellites. Ly$_\alpha$ line is the most intense spectral line containing about a half of all emitted photons. This makes this lin Ly$_\alpha$ line the best choice for quasi-monochromatic X-ray backlighter imaging and is sufficiently bright for use in appoint-project Bragg crystal

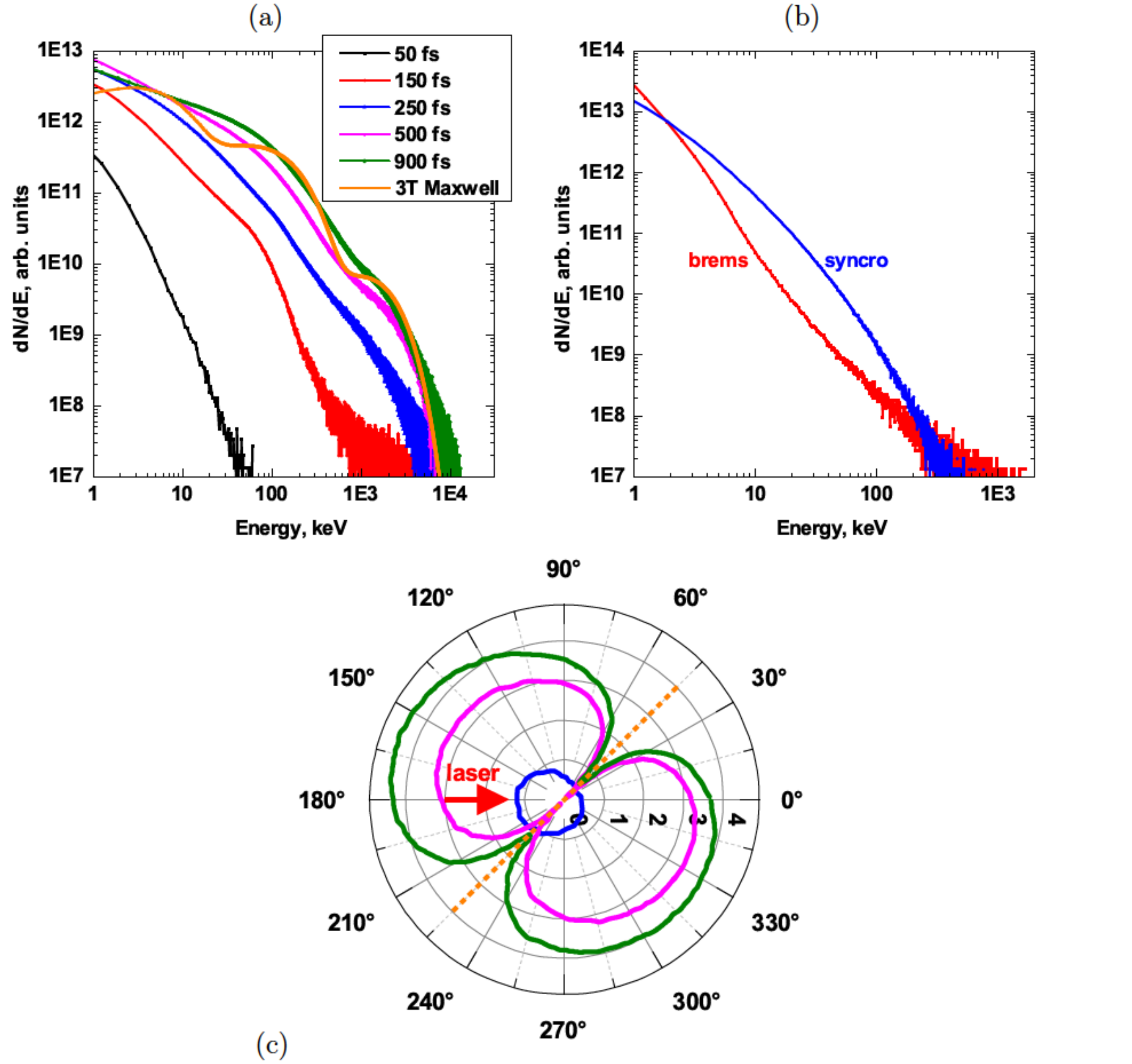

Figure 5. (a)—electron energy distribution retrieved from PIC simulations for different moments of the laser-target interaction; (b)—Spectra of bremsstrahlung and synchrotron emission retrieved from the PIC simulation; (c)—Numerically calculated angular distribution of bremsstrahlung (magenta curve) and synchrotron radiation (blue) emitted in the 4.8–7.3 Å (1.7–2.6 keV) wavelength range by a 2 μm thick layer of fully ionized Si ions with solid-state density irradiated by a subpicosecond laser pulse with intensity 3×10^{20} W/cm^2. The solid green curve is the sum of two components. The dashed green line represents the sum, when all the absorption processes were excluded from the simulations.

imaging system.

Emissivity of the source in continuous emission in direction close to the target normal is $\approx$13.6 mJ/sr (CE$\approx$0.7$\times10^{-4}$). $\approx$5 mJ/sr (CE $\approx$0.25$\times10^{-4}$) of it corresponds to free-free (bremsstrahlung and synctrotron) radiation. The rest is associated with recombination continuum emission. Such a high value of emissivity in such type of continous emission together with absence of spectral lines makes the investigated source very suitable for absorption spectroscopy purposes. The value of $CE_{4\pi}$ (a ratio between the energy emitted by the source in the full solid angle 4π and the energy of the laser pulse) in free-free emission estimated on the base of the simulated angular distribution and the experimentally measured emissivity is 1.6×10^{-4}. This is three times less than the value obtained directly from the code EPOCH. The difference of less than one order leads to the conclusion that the code reproduces processes at the interaction point quite well.

Acknowledgments

The work was performed in the period from December 2019 to August 2021. The authors would like to thank the Central Laser Facility staff, whose dedication and expertise were essential to the success of their experiment. Calculations were carried out on the computational resources of the JSCC RAS. The reported study was funded by RFBR, project number 19-32-60050. This study was done in the frame of the State Assignment to JIHT RAS (topic #075-00892-20-00). The work of UK team received financial support from UK EPSRC grants EP/P026796/1, EP/L01663X/1 and EP/H012605/1.

References

[1] J. Workman et al. "Picosecond soft-x-ray source from subpicosecond laser-produced plasmas". In: *Journal of the Optical Society of America B* 13.1 (Jan. 1996), p. 125. ISSN: 0740-3224. DOI: 10.1364/JOSAB.13.000125. URL: https://opg.optica.org/abstract.cfm?URI=josab-13-1-125.

[2] K. B. Wharton et al. "Effects of nonionizing prepulses in high-intensity laser-solid interactions". In: *Physical Review E* 64.2 (July 2001), p. 025401. ISSN: 1063-651X. DOI: 10.1103/PhysRevE.64.025401. URL: https://link.aps.org/doi/10.1103/PhysRevE.64.025401.

[3] D. Riley et al. "K_α yields from Ti foils irradiated with ultrashort laser pulses". In: *Physical Review E* 71.1 (Jan. 2005), p. 016406. ISSN: 1539-3755. DOI: 10.1103/PhysRevE.71.016406. URL: https://link.aps.org/doi/10.1103/PhysRevE.71.016406.

[4] M. M. Murnane et al. "Efficient coupling of high-intensity subpicosecond laser pulses into solids". In: *Applied Physics Letters* 62.10 (Mar. 1993), pp. 1068–1070. ISSN: 0003-6951. DOI: 10.1063/1.108797. URL: http://aip.scitation.org/doi/10.1063/1.108797.

[5] Subhendu Kahaly et al. "Near-Complete Absorption of Intense, Ultrashort Laser Light by Sub-λ Gratings". In: *Physical Review Letters* 101.14 (Sept. 2008), p. 145001. ISSN: 0031-9007. DOI: 10.1103/PhysRevLett.101.145001. URL: https://link.aps.org/doi/10.1103/PhysRevLett.101.145001.

[6] H. A. Sumeruk et al. "Control of Strong-Laser-Field Coupling to Electrons in Solid Targets with Wavelength-Scale Spheres". In: *Physical Review Letters* 98.4 (Jan. 2007), p. 045001. ISSN: 0031-9007. DOI: 10.1103/PhysRevLett.98.045001. URL: https://link.aps.org/doi/10.1103/PhysRevLett.98.045001.

[7] G. Kulcsár et al. "Intense Picosecond X-Ray Pulses from Laser Plasmas by Use of Nanostructured "Velvet" Targets". In: *Physical Review Letters* 84.22 (May 2000), pp. 5149–5152. ISSN: 0031-9007. DOI: 10.1103/PhysRevLett.84.5149. URL: https://link.aps.org/doi/10.1103/PhysRevLett.84.5149.

[8] A.V. Ovchinnikov et al. "Characteristic X-rays generation under the action of femtosecond laser pulses on nano-structured targets". In: *Laser and Particle Beams* 29.2 (June 2011), pp. 249–254. ISSN: 0263-0346. DOI: 10.1017/S026303461100022X. URL: https://www.cambridge.org/core/product/identifier/S026303461100022X/type/journal_article.

[9] Reed Hollinger et al. "Efficient picosecond x-ray pulse generation from plasmas in the radiation dominated regime". In: *Optica* 4.11 (Nov. 2017), p. 1344. ISSN: 2334-2536. DOI: 10.1364/OPTICA.4.001344. URL: https://opg.optica.org/abstract.cfm?URI=optica-4-11-1344.

[10] K. A. Schultz et al. "Study of pure and mixed clustered noble gas puffs irradiated with a high intensity (7 × 1019 W/cm2) sub-ps laser beam and achievement of a strong X-ray flash in a laser-generated debris-free X-ray source". In: *Laser and Particle Beams* 37.03 (Sept. 2019), pp. 276–287. ISSN: 0263-0346. DOI: 10.1017/S0263034619000521. URL: https://www.cambridge.org/core/product/identifier/S0263034619000521/type/journal_article.

[11] V.L. Kantsyrev et al. "Study of x-rays produced from debris-free sources with Ar, Kr and Kr/Ar mixture linear gas jets irradiated by UNR Leopard laser beam with fs and ns pulse duration". In: *High Energy Density Physics* 19 (June 2016), pp. 11–22. ISSN: 15741818. DOI: 10.1016/j.hedp.2016.02.001. URL: http://dx.doi.org/10.1016/j.hedp.2016.02.001%20https://linkinghub.elsevier.com/retrieve/pii/S1574181816300088.

[12] V. L. Kantsyrev et al. "Influence of Xe and Kr impurities on x-ray yield from debris-free plasma x-ray sources with an Ar supersonic gas jet irradiated by femtosecond near-infrared-wavelength laser pulses". In: *Physical Review E* 94.5 (Nov. 2016), p. 053203. ISSN: 2470-0045. DOI: 10.1103/PhysRevE.94.053203. URL: https://link.aps.org/doi/10.1103/PhysRevE.94.053203.

[13] G.-Y. Hu et al. "Angular distribution and conversion of multi-keV L-shell X-ray sources produced from nanosecond laser irradiated thick-foil targets". In: *Laser and Particle Beams* 26.4 (Dec. 2008), pp. 661–670. ISSN: 0263-0346. DOI: 10.1017/S0263034608000682. URL: https://www.cambridge.org/core/product/identifier/S0263034608000682/type/journal_article.

[14] R. Rathore et al. "Experimental and numerical study of ultra-short laser-produced collimated Cu K α X-ray source". In: *Laser and Particle Beams* 35.3 (Sept. 2017), pp. 442–449. ISSN: 0263-0346. DOI: 10.1017/S026303461700043X. URL: https://www.cambridge.org/core/product/identifier/S026303461700043X/type/journal_article.

[15] Carlo Kleine et al. "Soft X-ray Absorption Spectroscopy of Aqueous Solutions Using a Table-Top Femtosecond Soft X-ray Source". In: *The Journal of Physical Chemistry Letters* 10.1 (Jan. 2019), pp. 52–58. ISSN: 1948-7185. DOI: 10.1021/acs.jpclett.8b03420. URL: https://pubs.acs.org/doi/10.1021/acs.jpclett.8b03420.

[16] S. F. Khan et al. "A dual high-energy radiography platform with 15 μ m resolution at the National Ignition Facility". In: *Review of Scientific Instruments* 92.4 (Apr. 2021), p. 043712. ISSN: 0034-6748. DOI: 10.1063/5.0044043. URL: https://aip.scitation.org/doi/10.1063/5.0044043.

[17] A. Casner et al. "LMJ/PETAL laser facility: Overview and opportunities for laboratory astrophysics". In: *High Energy Density Physics* 17 (Dec. 2015), pp. 2–11. ISSN: 15741818. DOI: 10.1016/j.hedp.2014.11.009. URL: https://linkinghub.elsevier.com/retrieve/pii/S1574181814000871.

[18] *Opportunities in Intense Ultrafast Lasers*. Washington, D.C.: National Academies Press, Jan. 2018. ISBN: 978-0-309-46769-8. DOI: 10.17226/24939. URL: https://www.nap.edu/catalog/24939.

[19] T. C. Sangster et al. "Cryogenic DT and D2 targets for inertial confinement fusion". In: *Physics of Plasmas* 14.5 (May 2007), p. 058101. ISSN: 1070-664X. DOI: 10.1063/1.2671844. URL: http://aip.scitation.org/doi/10.1063/1.2671844.

[20] C. Stoeckl et al. "Soft x-ray backlighting of cryogenic implosions using a narrowband crystal imaging system (invited)". In: *Review of Scientific Instruments* 85.11 (Nov. 2014), 11E501. ISSN: 0034-6748. DOI: 10.1063/1.4890215. URL: http://aip.scitation.org/doi/10.1063/1.4890215.

[21] C. McGuffey et al. "Soft X-ray backlighter source driven by a short-pulse laser for pump-probe characterization of warm dense matter". In: *Review of Scientific Instruments* 89.10 (Oct. 2018), 10F122. ISSN: 0034-6748. DOI: 10.1063/1.5039419. URL: http://aip.scitation.org/doi/10.1063/1.5039419.

[22] A. S. Martynenko et al. "Optimization of a laser plasma-based x-ray source according to WDM absorption spectroscopy requirements". In: *Matter and Radiation at Extremes* 6.1 (Jan. 2021), p. 014405. ISSN: 2468-2047. DOI: 10.1063/5.0025646. URL: http://aip.scitation.org/doi/10.1063/5.0025646.

[23] B. Loupias et al. "Highly efficient, easily spectrally tunable X-ray backlighting for the study of extreme matter states". In: *Laser and Particle Beams* 27.4 (Dec. 2009), pp. 601–609. ISSN: 0263-0346. DOI: 10.1017/S0263034609990322.

URL: https://www.cambridge.org/core/product/identifier/S0263034609990322/type/journal_article.

[24] C.N Danson et al. "Vulcan Petawatt—an ultra-high-intensity interaction facility". In: *Nuclear Fusion* 44.12 (Dec. 2004), S239–S246. ISSN: 0029-5515. DOI: 10.1088/0029-5515/44/12/S15. URL: https://iopscience.iop.org/article/10.1088/0029-5515/44/12/S15.

[25] G G Scott et al. "Optimization of plasma mirror reflectivity and optical quality using double laser pulses". In: *New Journal of Physics* 17.3 (Mar. 2015), p. 033027. ISSN: 1367-2630. DOI: 10.1088/1367-2630/17/3/033027. URL: https://iopscience.iop.org/article/10.1088/1367-2630/17/3/033027.

[26] A. Ya Faenov et al. "High-Performance X-Ray Spectroscopic Devices for Plasma Microsources Investigations". In: *Physica Scripta* 50.4 (Oct. 1994), pp. 333–338. ISSN: 0031-8949. DOI: 10.1088/0031-8949/50/4/003. URL: http://iopscience.iop.org/article/10.1088/0031-8949/50/4/003/pdf%20http://stacks.iop.org/1402-4896/50/i=4/a=003?key=crossref.9f042b7c13029f622f645cd1b2fea7b2.

[27] Ya S Lavrinenko et al. "Reflectivity and imaging capabilities of spherically bent crystals studied by ray-tracing simulations". In: *Journal of Physics: Conference Series* 653.1 (Nov. 2015), p. 12027. ISSN: 17426596. DOI: 10.1088/1742-6596/653/1/012027. URL: http://stacks.iop.org/1742-6596/653/i=1/a=012027?key=crossref.64d2e6f480543d73c2219d620c1fd8c2%20http://stacks.iop.org/1742-6596/653/i=1/a=012027.

[28] Manuel Sánchez del Río and Roger J Dejus. "XOP v2.4: recent developments of the x-ray optics software toolkit". In: *Proc. SPIE*. Ed. by Manuel Sanchez del Rio and Oleg Chubar. Vol. 8141. Sept. 2011, p. 814115. ISBN: 0277-786X. DOI: 10.1117/12.893911. URL: http://proceedings.spiedigitallibrary.org/proceeding.aspx?doi=10.1117/12.893911.

[29] B.L. Henke, E.M. Gullikson, and J.C. Davis. "X-Ray Interactions: Photoabsorption, Scattering, Transmission, and Reflection at E = 50-30,000 eV, Z = 1-92". In: *Atomic Data and Nuclear Data Tables* 54.2 (July 1993), pp. 181–342. ISSN: 0092640X. DOI: 10.1006/adnd.1993.1013. URL: http://linkinghub.elsevier.com/retrieve/pii/S0092640X83710132.

[30] Dien Li et al. "Silicon K-edge XANES spectra of silicate minerals". In: *Physics and Chemistry of Minerals* 22.2 (Mar. 1995), pp. 115–122. ISSN: 0342-1791. DOI: 10.1007/BF00202471. URL: http://link.springer.com/10.1007/BF00202471.

[31] J. J. Macfarlane et al. "Simulation of the Ionization Dynamics of Aluminum Irradiated by Intense Short-Pulse Lasers". In: *Inertial Fusion Sciences and Applications 2003 (IFSA 2003): State of the Art 2003*. Ed. by B. A. Hammel et al. La Grange Park, IL: American Nuclear Society, 2004, p. 457.

[32] D. J. Hoarty et al. "Observations of the Effect of Ionization-Potential Depression in Hot Dense Plasma". In: *Physical Review Letters* 110.26 (June 2013), p. 265003. ISSN: 0031-9007. DOI: 10.1103/PhysRevLett.110.265003. URL: https://link.aps.org/doi/10.1103/PhysRevLett.110.265003.

[33] D. G. Hummer and Dimitri Mihalas. "The equation of state for stellar envelopes. I - an occupation probability formalism for the truncation of internal partition functions". In: *The Astrophysical Journal* 331 (Aug. 1988), p. 794. ISSN: 0004-637X. DOI: 10.1086/166600. URL: http://adsabs.harvard.edu/doi/10.1086/166600.

[34] T D Arber et al. "Contemporary particle-in-cell approach to laser-plasma modelling". In: *Plasma Physics and Controlled Fusion* 57.11 (Nov. 2015), p. 113001. ISSN: 0741-3335. DOI: 10.1088/0741-3335/57/11/113001. URL: https://iopscience.iop.org/article/10.1088/0741-3335/57/11/113001.

[35] Y.P. Raizer. *Gas Discharge Physics*. Ed. by J.E. Allen. Berlin: Springer Berlin, Heidelberg, 1991, p. 449. ISBN: 978-3-642-64760-4. URL: https://link.springer.com/gp/book/9783642647604.

[36] L D Landau and E.M. Lifshitz. *he Classical Theory of Fields: Volume 2*. Butterworth-Heinemann, 1985, p. 402.

[37] Jiří Vyskočil, Ondřej Klimo, and Stefan Weber. "Simulations of bremsstrahlung emission in ultra-intense laser interactions with foil targets". In: *Plasma Physics and Controlled Fusion* 60.5 (May 2018), p. 054013. ISSN: 0741-3335. DOI: 10.1088/1361-6587/aab4c3. URL: https://iopscience.iop.org/article/10.1088/1361-6587/aab4c3.

[38] R Duclous, J G Kirk, and A R Bell. "Monte Carlo calculations of pair production in high-intensity laser–plasma interactions". In: *Plasma Physics and Controlled Fusion* 53.1 (Jan. 2011), p. 015009. ISSN: 0741-3335. DOI: 10.1088/0741-3335/53/1/015009.

[39] N. V. Elkina et al. "QED cascades induced by circularly polarized laser fields". In: *Physical Review Special Topics - Accelerators and Beams* 14.5 (May 2011), p. 054401. ISSN: 1098-4402. DOI: 10.1103/PhysRevSTAB.14.054401.

[40] H.-S. Park et al. "Characteristics of high energy Kα and Bremsstrahlung sources generated by short pulse petawatt lasers". In: *Review of Scientific Instruments* 75.10 (Oct. 2004), pp. 4048–4050. ISSN: 0034-6748. DOI: 10.1063/1.1789596. URL: http://aip.scitation.org/doi/10.1063/1.1789596.

[41] H. S. Park et al. "High-energy Kα radiography using high-intensity, short-pulse lasers". In: *Physics of Plasmas* 13.5 (2006). ISSN: 1070664X. DOI: 10.1063/1.2178775.

[42] Michael J. Haugh et al. "Calibrating image plate sensitivity in the 700 to 5000 eV spectral energy range". In: *Proc. SPIE 8850, Target Diagnostics Physics and Engineering for Inertial Confinement Fusion II, (September 26, 2013)*. Ed. by Perry M. Bell and Gary P. Grim. Vol. 8850. Sept. 2013, p. 885007. ISBN: 9780819497000. DOI: `10.1117/12.2024889`. URL: `http://proceedings.spiedigitallibrary.org/proceeding.aspx?doi=10.1117/12.2024889`.

[43] D.O. Golovin et al. "Calibration of imaging plates sensitivity to high energy photons and ions for laser-plasma interaction sources". In: *Journal of Instrumentation* 16.02 (Feb. 2021), T02005–T02005. ISSN: 1748-0221. DOI: `10.1088/1748-0221/16/02/T02005`. URL: `http://www.pubmedcentral.nih.gov/articlerender.fcgi?artid=2734969&tool=pmcentrez&rendertype=abstract%20https://iopscience.iop.org/article/10.1088/1748-0221/16/02/T02005`.

[44] André Authier. *Dynamical Theory of X-Ray Diffraction*. Oxford University Press, Nov. 2003. ISBN: 9780198528920. DOI: `10.1093/acprof:oso/9780198528920.001.0001`. URL: `http://www.oxfordscholarship.com/view/10.1093/acprof:oso/9780198528920.001.0001/acprof-9780198528920`.

Appendix A. Recalculation of raw data counts to number of real photons

Raw data recorded by the Fuji BAS TR Image Plates (IPs below) detectors in the experiments is a two-dimensional matrix of numbers. Each of them is proportional to a dose absorbed by a certain pixel of the detector. This matrix can be represented in a form of a grayscale image shown in Fig. A1. The spectrum is a profile along the bright narrow field in the centre of the image. This zone has a non-zero width in pixels, so each dot of the spectrum is a sum along the vertical axis.

The data from IPs were digitized via Fujifilm FLA 5100 scanner. A raw image produced as a result of scanning is scaled in arbitrary units (counts), which are related with absolute units called PSL (Photostimulated Luminescence) by the equation A.1 [42]:

$$PSL = \left(\frac{R}{100}\right)^2 \left(\frac{400}{S}\right) 10^{L\left(\frac{G}{2^B-1}-\frac{1}{2}\right)}, \tag{A.1}$$

where R is the resolution in microns, S is a sensitivity setting, L is latitude, B is a dynamic range in bits, G is the raw image grayscale value, which is sometimes mentioned as a quantum yield. We used the following values for scanning: $R = 25$, $S = 5000$, $L = 5$, $B = 16$. It should be noted that the counts-to-PSL recalculation function can be significantly different for other scanner models. For example, for General Electric Typhoon FLA 7000 the equation can be found in [43]. The values in PSL were recalculated to a number of photons with a given wavelength on the base of a calibration curve shown in Fig. A2.

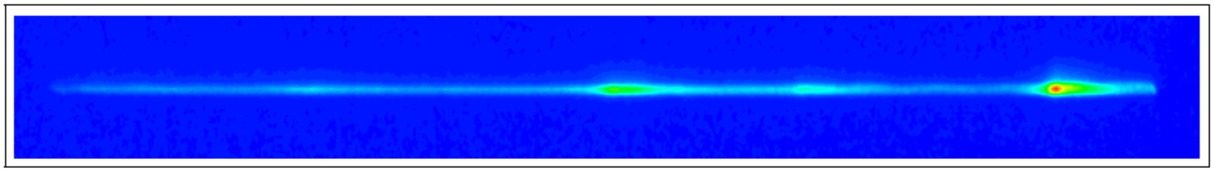

Figure A1. An example of an experimental X-ray emission spectrum registered by the IP detector installed in the FSSR.

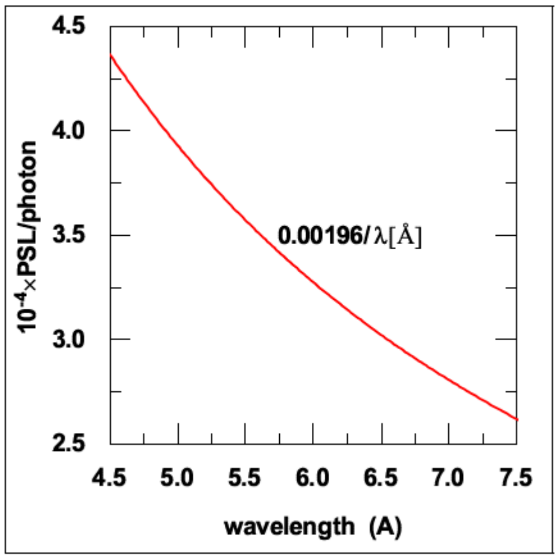

Figure A2. Sensitivity of Fuji BAS TR IPs in the soft X-ray range from [42] fitted by a hyperbola function.

Appendix B. Crystal reflectivity

The corrections associated with Crystal Reflectivity (CR) were also considered during spectra restoring process. The CR function here is N_r/N_e, where N_r and N_e are numbers of photons reflected by a crystal and emitted by a source, correspondingly. It depends on a solid angle covered by the spectrometer crystal (Ω_{cr}) and also on its rocking curves (diffraction profiles). Ω_{cr} was calculated directly from the distance between the source and the crystals and the surface dimensions of the latter ones. Rocking curves were obtained by the X-ray Oriented Programs (XOP) [28]. This software allowed to simulate diffraction properties of spherically-bent crystals on the base of extended dynamical theory, which is fully described, for example, in [44]. The calculated rocking curves are shown in Fig. B1. The curves were taken into account in a numerical simulation (modelling principles are described in [27]) of rays propagation through the spectrometers optical schemes. They were considered as profiles of probability for a photon with given energy and incidence angle to be reflected by spherically bent crystals of the FSSRs.

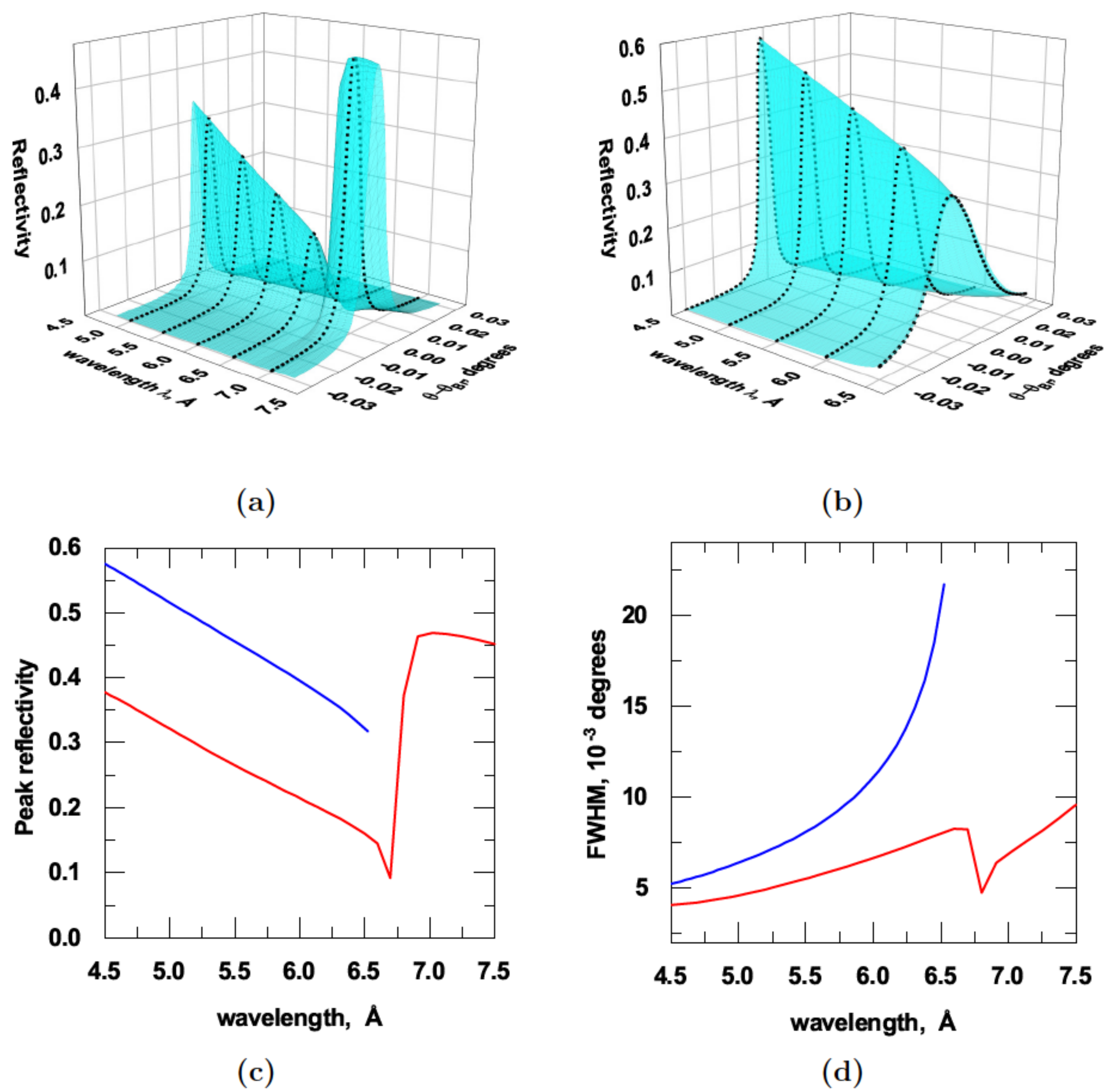

Figure B1. Set of rocking curves presented as a 3D surface calculated by the XOP software for spherically bent α-quartz crystals with Miller indexes **(a)** (100) and **(b)** (101) for the range of wavelengths observed in the experiments. For (101) the data is not presented for $\lambda > 6.666$ Å, because the crystal is not able to reflect photons with a wavelength longer than its interplanar spacing 2d = 6.666 Å. Dependence of the peaks amplitude (peak reflectivity for a particular wavelength) and FWHM are given on the planes **(c)** and **(d)** correspondingly: red line for (100), blue line for (101).